

A129088

AD

TECHNICAL REPORT ARBRL-TR-02488

EIGENFREQUENCIES OF INERTIAL  
OSCILLATIONS IN A ROTATING FLUID VIA A  
NUMERICAL SIMULATION

Raymond Sedney  
Nathan Gerber  
Joan M. Bartos

May 1983



US ARMY ARMAMENT RESEARCH AND DEVELOPMENT COMMAND  
BALLISTIC RESEARCH LABORATORY  
ABERDEEN PROVING GROUND, MARYLAND

Approved for public release; distribution unlimited.

Destroy this report when it is no longer needed.  
Do not return it to the originator.

Additional copies of this report may be obtained  
from the National Technical Information Service,  
U. S. Department of Commerce, Springfield, Virginia  
22161.

The findings in this report are not to be construed as  
an official Department of the Army position, unless  
so designated by other authorized documents.

*The use of trade names or manufacturers' names in this report  
does not constitute indorsement of any commercial product.*

UNCLASSIFIED

SECURITY CLASSIFICATION OF THIS PAGE (When Data Entered)

REPORT DOCUMENTATION PAGE		READ INSTRUCTIONS BEFORE COMPLETING FORM
1. REPORT NUMBER TECHNICAL REPORT ARBRL-TR-02488	2. GOVT ACCESSION NO.	3. RECIPIENT'S CATALOG NUMBER
4. TITLE (and Subtitle) EIGENFREQUENCIES OF INERTIAL OSCILLATIONS IN A ROTATING FLUID VIA A NUMERICAL SIMULATION		5. TYPE OF REPORT & PERIOD COVERED Final
		6. PERFORMING ORG. REPORT NUMBER
7. AUTHOR(s) Raymond Sedney Nathan Gerber Joan M. Bartos		8. CONTRACT OR GRANT NUMBER(s)
9. PERFORMING ORGANIZATION NAME AND ADDRESS US Army Ballistic Research Laboratory ATTN: DRDAR-BLL Aberdeen Proving Ground, Maryland 21005		10. PROGRAM ELEMENT, PROJECT, TASK AREA & WORK UNIT NUMBERS RDT&E 1L161102AH43
11. CONTROLLING OFFICE NAME AND ADDRESS US Army Armament Research & Development Command US Army Ballistic Research Laboratory (DRDAR-BLA-S) Aberdeen Proving Ground, Maryland 21005		12. REPORT DATE May 1983
		13. NUMBER OF PAGES 45
14. MONITORING AGENCY NAME & ADDRESS (if different from Controlling Office)		15. SECURITY CLASS. (of this report)  UNCLASSIFIED
		15a. DECLASSIFICATION/DOWNGRADING SCHEDULE
16. DISTRIBUTION STATEMENT (of this Report)  Approved for public release, distribution unlimited.		
17. DISTRIBUTION STATEMENT (of the abstract entered in Block 20, if different from Report)		
18. SUPPLEMENTARY NOTES		
19. KEY WORDS (Continue on reverse side if necessary and identify by block number) <div style="display: flex; justify-content: space-between;"> <div>           Rotating Fluid            Inertial Oscillations            Eigenfrequencies            Numerical Simulation         </div> <div>           Linear Eigenvalue Theory            Fourier Transform and Digital Filter            Preprocessing         </div> <div style="color: red; font-style: italic;">           Two files per            fluid mech         </div> </div>		
20. ABSTRACT (Continue on reverse side if necessary and identify by block number) (bja) <p>An understanding of the instability of a spinning liquid-filled projectile requires a knowledge of the wave system in the rotating fluid. The axisymmetric wave system in a cylinder is studied by a numerical simulation; the particular case of perturbed solid body rotation is treated. Finite-difference solutions to the Navier-Stokes equations provide data from which wave frequencies and damping can be extracted using Fourier transform and</p>		

UNCLASSIFIED

SECURITY CLASSIFICATION OF THIS PAGE (When Data Entered)

UNCLASSIFIED

SECURITY CLASSIFICATION OF THIS PAGE(When Data Entered)

digital filter techniques. The frequency and damping are compared with the values computed from a linearized eigenvalue analysis. It is found that the latter can be used with confidence for Reynolds number as low as 1,000.

UNCLASSIFIED

SECURITY CLASSIFICATION OF THIS PAGE(When Data Entered)

## TABLE OF CONTENTS

	<u>Page</u>
LIST OF ILLUSTRATIONS.....	5
I. INTRODUCTION.....	7
II. THE LINEAR THEORY WITH CORRECTION.....	10
III. FINITE DIFFERENCE SOLUTION TO NAVIER-STOKES EQUATIONS FOR A ROTATING CYLINDER.....	11
IV. ANALYSIS OF THE DATA.....	13
V. RESULTS.....	17
VI. CONCLUSIONS.....	18
ACKNOWLEDGMENTS.....	18
REFERENCES.....	30
APPENDIX A.....	31
LIST OF SYMBOLS.....	37
DISTRIBUTION LIST.....	39

# LIST OF ILLUSTRATIONS

<u>Figure</u>		<u>Page</u>
1	Cylinder, Coordinates, and Notation.....	19
2	Typical Pressure History - $\Delta p_1$ vs $t$ for Perturbed Solid Body Rotation with Single Mode Excitation ( $Re =$ $1.0 \times 10^3$ , $c/a = 1.0$ , $\epsilon = 0.05$ , $\omega = 1.15$ , $t_c = 70.375$ ).....	19
3	Amplitude Response Curve - $\max  \Delta p $ vs Forcing Frequency ( $c/a = 1.0$ , $\epsilon = 0.05$ ).....	20
4	Instantaneous Meridional Streamlines for Four Perturbation Frequencies ( $Re = 1 \times 10^4$ , $c/a = 1.0$ , $\epsilon = 0.05$ ).....	21
5	Pressure History, $\Delta p_1$ After Cut-Off for a Case With Two Dominant Modes ( $Re = 1.0 \times 10^3$ , $c/a =$ $1.0$ , $\epsilon = 0.05$ , $\omega = 0.88$ , $t_c = 67.875$ ).....	23
6	Fourier Transform of the Pressure History Shown in Figure 5 ( $Re = 1.0 \times 10^3$ , $c/a = 1.0$ , $\epsilon = 0.05$ ).....	23
7	Band Pass Filter of the Pressure History Shown in Figure 5 ( $Re = 1.0 \times 10^3$ , $c/a = 1.0$ , $\epsilon = 0.05$ , $t_c =$ $67.875$ , $0.11 \leq \nu_f \leq 0.15$ ).....	24
8	Comparison of Fourier Transforms (a) Before and (b) After Preprocessing the Data ( $Re = 100.0$ , $c/a = 1.0$ , $\epsilon = 0.05$ , $\omega = 0.83$ , $t_c = 40.0$ , $40.0 \leq t \leq 53.0$ , $\bar{\alpha}_{21} = 0.3$ ).....	25
9	Comparison of Eigenfrequencies From Linear Theory With Correction, $C_R$ , and Those From Numerical Simulation, $f$ ( $c/a = 1.0$ , $k = 2$ ).....	26
10	Comparison of Wave Dampings From Linear Theory, $C_I$ , With Those From Numerical Simulation, $\alpha$ , and From Kudlick Theory ( $c/a = 1.0$ , $k = 2$ ).....	27
11	Comparison of Eigenfrequencies From Linear Theory With Correction, $C_R$ , and Those From Numerical Simulation, $f$ ( $c/a = 1.0$ , $k = 4$ ).....	28
12	Comparison of Wave Dampings From Linear Theory, $C_I$ , With Those From Numerical Simulation, $\alpha$ , and From Kudlick Theory ( $c/a = 1.0$ , $k = 4$ ).....	29

## I. INTRODUCTION

A liquid payload in a spinning projectile can cause the projectile to be unstable for certain combinations of parameters of the system, even though the same projectile with a solid payload is stable. An understanding of this phenomenon requires a knowledge of the wave system in the rotating fluid. The ability to support waves is a fundamental property of a rotating fluid. The angular motion of the projectile excites these waves, often called inertial waves. In this study a numerical experiment generates data that are used to validate a linear theory for waves in a rotating fluid contained in a cylinder.

Only linear theories are available to analyze the effects of a liquid payload on the flight of a spinning projectile. The two main goals of such theories are: (1) Calculate the moment exerted by the liquid and thereby determine the rate of growth of the projectile yaw. (2) Calculate the frequencies and damping of the predominant modes of oscillation of the rotating fluid. For a cylinder containing a liquid in solid-body rotation, an inviscid theory which met these goals was presented by Stewartson,<sup>1</sup> and a significant improvement on this was made by Wedemeyer,<sup>2</sup> who derived viscous corrections. Reference 3 presents a technique for achieving (2) for a liquid in the unsteady spin-up process or in solid body rotation; results are given there only for the latter case.

To accomplish (2), the first step is to linearize the Navier-Stokes equations. A small perturbation about a basic state, solid-body rotation or spin-up, is assumed, and these perturbations are analyzed into modes. The solution to the eigenvalue problem thus defined yields the complex eigenvalue\*  $C = C_R + iC_I$  where  $C_R$  and  $C_I$  are the frequency and damping of the wave, respectively. With a modal analysis, the no-slip boundary conditions on the

---

\*Definitions of terms are given in List of Symbols, p. 37.

1. K. Stewartson, "On the Stability of a Spinning Top Containing Liquid," J. Fluid Mech., Vol. 5, Part 4, September 1959, pp. 577-592.
2. E. H. Wedemeyer, "Viscous Corrections to Stewartson's Stability Criterion," BRL Report No. 1325, Aberdeen Proving Ground, Maryland, June 1966 (AD 489687). Also "Dynamics of Liquid-Filled Shell: Theory of Viscous Corrections to Stewartson's Stability Problem," BRL Report No. 1287, June 1965 (AD 472474).
3. C. W. Kitchens, Jr., N. Gerber, and R. Sedney, "Oscillations of a Liquid in a Rotating Cylinder: Part I. Solid Body Rotation," Technical Report ARBRL-TR-02081, June 1978 (AD A057759).



end walls cannot be satisfied; only the normal component of velocity vanishes there. The effect of using the "inviscid type" boundary conditions on the end wall is to cause an error in  $C_R$  of, at most, a few percent; the error in  $C_I$  can be more than a factor of 2. Therefore, a correction for  $C$  is required.

Such a correction is derived in Reference 3 for perturbed solid-body rotation. Although it is different in detail from that derived by Wedemeyer,<sup>2</sup> the necessary analysis proceeds in much the same way. The attempts in References 3 and 4 to validate the linear eigenvalue theory by comparison with experimental data were not definitive. Validation of this theory is the primary objective of this report.

Recently, a finite difference technique to solve the Navier-Stokes equations for the fluid motion in a rotating cylinder was presented by Kitchens.<sup>5</sup> The original objective of the work was to study the axisymmetric spin-up problem. Since this technique is accurate and reliable, it provides solutions where the accuracy is limited only by the grid sizes. Being restricted to axisymmetric flow, this technique can only yield results for azimuthal wave number  $m = 0$ . For the projectile case, however,  $m = 1$  is the wave number of interest. We believe that the conclusions we reach on the validity of the linear theory for  $m = 0$  will be a useful guide for the  $m = 1$  case. Therefore, we shall use the technique of Reference 5 to generate data with which to validate the linear theory.

Experimental data for  $m = 0$  were obtained by Aldridge;<sup>6</sup> however, a systematic error exists in the reduction of the data to frequency. Recently, Aldridge and Stergiopoulos<sup>7</sup> used a different reduction method and the switch-

- 
4. R. D. Whiting and N. Gerber, "Dynamics of a Liquid-Filled Gyroscope: Update of Theory and Experiment," Technical Report ARBRL-TR-02221, March 1980 (AD A083886).
  5. C. W. Kitchens, Jr., "Navier-Stokes Solutions for Spin-Up in a Filled Cylinder," *AIAA Journal*, Vol. 18, No. 8, August 1980, pp. 929-934. Also Technical Report ARBRL-TR-02193, September 1979 (AD A077115).
  6. K. D. Aldridge, "Experimental Verification of the Inertial Oscillations of a Fluid in a Cylinder During Spin-Up," BRL Contract Report No. 273, Aberdeen Proving Ground, Maryland, September 1975 (AD A018797). Also *Geophys. Astrophys. Fluid Dynamics*, Vol. 8, 1977, pp. 279-301.
  7. K. D. Aldridge and S. Stergiopoulos, "Recovery of Complex Eigenfrequencies of Inertial Waves by Linearized Inversion of Viscous Decay Records," to be submitted for publication. See also S. Stergiopoulos, "An Experimental Study of Inertial Waves in a Fluid Contained in a Rotating Cylindrical Cavity During Spin-Up From Rest," Ph.D Thesis, York University, Toronto, Ontario, February 1982.



off technique, to be described later, and obtained frequencies that agree with our numerical simulation results. In these experiments and our finite difference solutions the small perturbation is a sinusoidal oscillation of the angular velocity of the cylinder. Only perturbed solid-body rotation is reported here; spin-up cases have been done and will be reported separately.

Previous experimental determinations of the frequencies were reported by Fultz,<sup>8</sup> using an oscillating disk on the axis of the cylinder to excite the waves and dye to observe the fluid motion. For a range of values of cylinder height to radius, but for essentially only one Reynolds number, he found that the frequencies agreed closely with those from inviscid theory. The theoretical study by Kudlick<sup>9</sup> gave viscous corrections to the inviscid results and expressions for the wave damping; see Section V for further discussion of this theory. The work of Kudlick<sup>9</sup> and Fultz<sup>8</sup> is discussed by Greenspan.<sup>10</sup>

One of the main considerations in our work is how to analyze the data from the finite difference solution. Following Aldridge, we use pressure differences on the axis versus time as our diagnostic. Of the doubly infinite set of inertial waves generated by the perturbation, the lower modes are most pertinent. If the damping is small and the modes are well separated, we can use the same methods for analyzing the data as are used for other continuous systems, which are based on simple harmonic oscillator concepts. For several modes these conditions were not satisfied, and for these cases it was necessary to use Fourier transform and digital filter methods. For  $Re = O(10^2)$ , where  $Re$  = Reynolds number, the damping in the system was so large that preprocessing of the pressure data was necessary.

From the finite difference solutions to the Navier-Stokes equations, the frequency and damping were obtained for several modes at  $Re = 10^2, 10^3$ , and  $10^4$ , mostly for aspect ratio unity. For the two higher  $Re$ , the frequency agreed with  $C_R$  to within  $\pm 2\%$  for the  $k = 2$  mode and  $\pm 3.5\%$  for the  $k = 4$  mode (mode index  $k$  is defined in (1) and (2)). The damping agreed with  $C_I$  to within  $\pm 5\%$  for  $k = 2$  and  $\pm 6.5\%$  for  $k = 4$ . It appeared that closer agreement with  $C_I$  could have been obtained if the accuracy of the finite difference solution were increased by decreasing grid sizes. Since the correction for  $C$  is of a boundary-layer type, its validity should deteriorate as  $Re$  decreases;

- 
8. D. Fultz, "A Note on Overstability and the Elastoid-Inertia Oscillations of Kelvin, Solberg, and Bjerkness," J. Meteorology, Vol. 16, April 1959, pp. 199-208.
  9. M. D. Kudlick, "On the Transient Motion of a Contained Rotating Fluid," Ph.D. Thesis, Massachusetts Institute of Technology, 1966.
  10. H. P. Greenspan, The Theory of Rotating Fluids, Cambridge University Press, New York, NY, 1968, pp. 81ff.

at the lowest  $Re$ , larger discrepancies were obtained. The conclusion is that the linear theory with correction can be used with confidence for  $Re$  as low as 1,000.

## II. THE LINEAR THEORY WITH CORRECTION

A brief outline of the theory will be given, mainly to introduce notation and concepts; see Reference 3 for details. The unperturbed container spin rate is  $\Omega_0$ ;  $a$  is the container radius and  $a \cdot c$  is its half-height;  $\nu$  is the liquid kinematic viscosity. Length, velocity, pressure, and time are non-dimensionalized by  $a$ ,  $a\Omega_0$ ,  $\rho\Omega_0^2 a^2$ , and  $1/\Omega_0$ , respectively, where  $\rho$  is the liquid density. Dimensionless nonrotating cylindrical coordinates  $r$ ,  $\theta$ , and  $z$  are used, with  $z = 0$  at one endwall; dimensionless time is denoted by  $t$ . The coordinates and some symbols are defined in Figure 1. We perturb about a basic flow of solid-body rotation given by

$$U = 0, \quad V = r, \quad W = 0, \quad \partial P / \partial r = r,$$

where  $U$ ,  $V$ , and  $W$  are radial, azimuthal, and axial velocity components, respectively, and  $P$  is pressure.

The perturbation pressure,  $\bar{p}$ , and velocities,  $\bar{u}$ ,  $\bar{v}$ ,  $\bar{w}$  in the  $r$ ,  $\theta$ ,  $z$  directions, satisfy the linearized Navier-Stokes equations. At this stage there is no restriction on Reynolds number

$$Re = \Omega_0 a^2 / \nu$$

unless the basic flow requires one. For solid-body rotation there is no restriction. We assume that the perturbation can be represented as a superposition of modes:

$$\bar{u} = \hat{u}(r) \cos Kz \exp [i (Ct - m\theta)] \quad (1a)$$

$$\bar{v} = \hat{v}(r) \cos Kz \exp [i (Ct - m\theta)] \quad (1b)$$

$$\bar{w} = \hat{w}(r) \sin Kz \exp [i (Ct - m\theta)] \quad (1c)$$

$$\bar{p} = \hat{p}(r) \cos Kz \exp [i (Ct - m\theta)] \quad (1d)$$

where

$$K = k\pi / (2c). \quad (2)$$

In this form the disturbances are complex, the real parts being the physical quantities; also the functions  $\hat{u}(r)$ ,  $\hat{v}(r)$ ,  $\hat{w}(r)$ , and  $\hat{p}(r)$  are complex. The integers  $m = 0, \pm 1, \dots$ , and  $k = 1, 2, \dots$  are azimuthal and axial wave numbers, respectively, and  $C \equiv C_R + i C_I$  is the eigenvalue. All quantities are

dimensionless. The natural frequency is equal to  $C_R \Omega_0$  and the decay rate of the disturbance is equal to  $C_I \Omega_0$  in dimensional form. A radial wave number,  $n$ , is determined by the functions of  $r$ . Since the numerical simulation employed here requires  $m = 0$  (axisymmetric disturbance), the modes can be identified by the pair of integers  $(k, n)$ . The corresponding values of  $C_R$  and  $C_I$  are designated with the subscripts  $k, n$ .

The functions of  $r$  satisfy a 6-th order system (complex) of ordinary differential equations which, together with homogeneous boundary conditions at  $r = 0$  and  $r = 1$ , define the eigenvalue problem. The no-slip boundary conditions are satisfied at the side wall,  $r = 1$ . Since the equations have a singularity at  $r = 0$ , the form of the solution is determined analytically near  $r = 0$ ; the boundary conditions there must be derived on the basis of continuity and single-valuedness. For  $Re > 0(10^3)$  special care is required in the numerical integration. The process of orthonormalization is used to cope with the phenomena of growing solutions and loss of linear independence.

The boundary conditions at the end walls ( $z = 0, 2c$ ) are  $\bar{u}^* = \bar{v}^* = \bar{w}^* = 0$ . The modal decomposition form assumed in (1) allows only the condition  $\bar{w}^* = 0$  to be satisfied; the no-slip condition on the end walls,  $\bar{u}^* = \bar{v}^* = 0$ , is not satisfied. To account for this a boundary-layer type of correction is made to the solution; it is described in Reference 3.

The correction is essentially a solution to the perturbation boundary layer equations. The boundary layer is introduced to correct for the neglect of the no-slip boundary conditions at the end walls. From the solution of these boundary layer equations a complex displacement thickness,  $\delta c$ , is determined. The  $K$  of (2) is replaced by  $K_c = (k\pi/2)/(c - \delta c)$ . The eigenvalue problem is solved again to yield the corrected  $C$ . The solution to the perturbation boundary-layer equations is correct to  $O(Re^{-1/2})$ ; therefore, a restriction to "large"  $Re$  now exists.

Two questions can be raised: (1) Is the corrected  $C$  adequate for present application. (2) What is the lower limit on  $Re$  for a given accuracy of  $C$ ? Ordinarily, one would seek experimental results to answer these questions. However, there was a scarcity of experimental data at the time of the early computations of  $C$ . The available measurements of Aldridge<sup>6</sup> consisted only of frequency  $C_R$ , mainly for spin-up, and the range of parameters in his experiments was not sufficient for our purposes. Therefore, we resorted to a numerical simulation to obtain frequency and damping with which  $C$  could be compared.

### III. FINITE DIFFERENCE SOLUTION TO NAVIER-STOKES EQUATIONS FOR A ROTATING CYLINDER

Kitchens<sup>5</sup> developed a finite difference technique for solving the Navier-Stokes equations for axisymmetric flow in a rotating cylinder. This solution was set up especially for the spin-up flow but can be adapted to other flows by changing the boundary and/or initial conditions. Because of the special problem considered in Reference 5, symmetry about the midplane,  $z = c$ , was

assumed; this restriction can easily be removed but will be retained here; thus, only even k modes are possible.

Coordinate transformations allow concentration of grid points near the boundaries. A stability criterion giving the allowable step size,  $\Delta t$ , is tested at each step of the calculation. Seven other parameters determine the convergence and accuracy of the solution: the numbers of points in the r and z directions, relaxation constants for each of the three dependent variables, and two coordinate stretching constants. This method has proved to be accurate and reliable. For spin-up from rest, convergence was obtained for Re up to  $5 \times 10^4$  with moderate computation time; convergence was not achieved for Re =  $10^5$ . For the perturbation problem calculations for larger Re have been made.

Since we wished to validate linear theory, calculations were made with a small perturbation on solid body rotation. The time history of angular velocity prescribed for the cylinder is

$$\begin{aligned}\Omega(t)/\Omega_0 &= 1 & t \leq 0 \\ &= 1 + \epsilon \sin \omega t & 0 \leq t \leq t_c \\ &= 1 & t > t_c\end{aligned}$$

For a range of values of  $\epsilon$  near  $\epsilon = 0.05$  it was verified that the solution depended linearly on  $\epsilon$ . The forcing function  $\Omega(t)$  induces a wave-type response in the fluid. The velocity components, pressure, and stream function, which are computed at all grid points, are available to analyze the response. A choice must be made as to the flow variable and the particular aspect of its variation to be used in extracting the wave parameters.

A physically significant diagnostic is the pressure difference on the axis of the cylinder. A derivation of the formula for pressure,  $p(r,z,t)$  is given in the Appendix. In the experiments of Aldridge two pressure differences

$$\Delta p_1 = p(0, c, t) - p(0, 0, t)$$

and

$$\Delta p_{1/2} = p(0, c/2, t) - p(0, 0, t)$$

were used to extract data for  $k = 2$  and  $k = 4$ , respectively. In the reduction of our data it was found that  $\Delta p_{1/2}$  did not clearly separate  $k = 2$  and  $k = 4$ . However,

$$\Delta p_a = 0.5 \Delta p_1 - \Delta p_{1/2}$$

effectively separates  $k = 4$ . The reason for this can be seen if it is assumed that the pressure at  $r = 0$  can be expanded in a series of eigenfunctions obtained from (1):

$$p(0, z, t) = \sum_{\substack{k = 2, 4, \dots \\ n = 1, 2, \dots}} A_{kn} \cos Kz \exp (iC_{kn} t) \quad (3)$$

where  $A_{kn}$  are constant coefficients. From this

$$\Delta p_1 = -2 \sum_n A_{2n} \exp (iC_{2n} t) + \dots \quad (4)$$

$$\Delta p_{1/2} = - \sum_n A_{2n} \exp (iC_{2n} t) - 2 \sum_n A_{4n} \exp (iC_{4n} t) + \dots \quad (5)$$

$$\Delta p_a = 2 \sum_n A_{4n} \exp (iC_{4n} t) + \dots \quad (6)$$

are obtained, where the omitted terms start with  $k = 6$ . It is clear from these expressions why  $\Delta p_{1/2}$  does not separate out the  $k = 4$  mode whereas  $\Delta p_a$  does; this is most evident if  $C_{21} = C_{41}$ .

An example of the time history of  $\Delta p_1$  is shown in Figure 2. The analysis of such records, which yields the frequency and damping of the inertial waves, is discussed next.

#### IV. ANALYSIS OF THE DATA

The response,  $\Delta p_1$  vs  $t$ , illustrated in Figure 2 is simple enough so that ideas from simple harmonic oscillator analysis can be used; for this case  $\epsilon = 0.05$ ,  $\omega = 1.25$ ,  $t_c = 70.4$ . The transient response, caused by initiating the perturbation, lasts until about  $t \approx 50$  and the steady-state response exists for  $50 < t < t_c = 70.4$ . For  $t > t_c$  the free response decays approximately exponentially. The step size in this example is  $\Delta t = 0.125$  so that there are forty or more points per cycle of response; in all cases this number was never less than twenty.

Amplitude response curves, obtained by plotting  $\max |\Delta p_1|$  and  $\max |\Delta p_a|$  of the steady state vs  $\omega$ , are shown in Figure 3 for  $Re = 1.0 \times 10^3$  and  $1.0 \times 10^4$ , and  $c/a = 1.0$ . The nondimensional flow solution is completely characterized by  $Re$  and  $c/a$ . The values of  $\omega$  at the peaks on the curves,  $\omega_m$ , approximate the frequencies of inertial oscillations,  $f_{kn}$ ; the values of  $n$  increase from  $n = 1$  as  $\omega_m$  decreases. From simple harmonic oscillator analysis the error in determining  $f_{kn}$  from the peak location is



$$(f_{kn} - \omega_m)/f_{kn} \approx (\alpha_{kn}/f_{kn})^2$$

where  $\alpha_{kn}$  is the damping of the  $(k, n)$  mode. The sharp peaks have small values of  $\alpha_{kn}/f_{kn}$ . For  $Re = 1.0 \times 10^3$  the second peak for  $k = 2$  is not well defined, and the  $k = 4$  curve has no peaks;  $f$  cannot be determined from the amplitude response curves in these cases.

For the type of time response illustrated in Figure 2, the damping,  $\alpha_{21}$ , can be determined from the logarithmic decrement of the peaks of the free response for  $t > t_c$ . If, however, two or more modes are mixed in the free response, the above method cannot by itself be used to determine  $\alpha$ . The presence of two mixed modes can be surmised from the pressure histories; a definite indication can be obtained by plotting the instantaneous streamlines. Since this is a more time-consuming process, it is not done routinely.

These are shown in Figure 4 for  $Re = 10^4$ ,  $c/a = 1$ ,  $\epsilon = 0.05$  at four values of  $\omega$ . In Figures 4a and 4c  $\omega \approx \omega_m$  in the amplitude response curve for  $k = 2$  in Figure 3, and well-defined cells are plotted for  $n = 3$  and  $n = 2$ , respectively, showing the presence of single modes. In Figure 4b  $\omega = 0.7$ , a value between two peaks of the amplitude response curve. As expected, well-defined cells are not obtained, showing the presence of mixed modes. In Figure 4d  $\omega = 1.05$ , which is near a minimum in the  $k = 2$  and a maximum in the  $k = 4$  amplitude response curves, and well-defined cells are obtained for the  $k = 4$ ,  $n = 3$  mode.

For  $Re = 10^3$  a  $\Delta p_1$  vs  $t$  response with two modes present in the free response is given in Figure 5. Only the response after cutoff,  $t > t_c = 67.875$ , is used in the analysis. The parameters other than  $t_c$  for Figure 5 are the same as those for Figure 2 except that  $\omega = 0.38$ , which is the value of  $\omega_m$  at the broad maximum in the  $\Delta p_1$  curve in Figure 3 for  $Re = 10^3$ . The lack of a sharp peak indicates that the elementary method may fail.

Figure 5 suggests that there are two or more modes mixed in the transient response data, and this is verified by the Fourier transform of this data shown in Figure 6. The magnitude of the transform,  $|F|$ , is plotted vs the frequency,  $\nu_f$ , in Hz. The dimension of  $\nu_f$  assumes that  $\Omega = 1$  rad/s. A fast Fourier transform computer program is used to calculate  $|F|$ . In obtaining  $|F|$  for this case, data from  $67.875 \leq t \leq 125.0$  are used, giving 458 points. The program requires a number of points equal to a power of 2; to obtain a convenient interval  $\Delta \nu_f$  for calculating  $|F|$ , zeros are added to the sequence of data points to give 4,096 points. The transform is shown in Figure 6 for  $\nu_f < 0.4$  Hz, although it was calculated for  $0 < \nu_f < 4.0$  Hz; the part beyond 0.4 Hz is of no interest.

Aside from the solution to the Navier-Stokes equations, the Fourier transform depends on the number of data points and their location in the

complete data set. Deleting points from the end of the interval has little effect on  $|F|$ , but deleting points at the beginning may have a noticeable effect. If the data starts at  $t = t_c$ , it may contain enough of the steady-state response so that  $\omega$  appears in the spectrum or influences it. If the initial data point is several time units greater than  $t_c$  and there is a mode with relatively large damping, that mode may not appear in the spectrum or it may be distorted. In our treatment the optimum choice of initial point was determined empirically. If the initial point for the example in Figure 6 is taken to be  $t = 75.5$ , the general shape of the curve is the same and the two frequencies in the spectrum are unchanged, but  $|F|$  is reduced by a factor of 3, and some additional small peaks appear.

To obtain an accurate value of the higher frequency in the spectrum, an  $\omega$  closer to  $f_{21}$  than to  $f_{22}$  should be used to generate the data; an initial guess can be obtained from inviscid theory. Then  $f_{22}$  is obtained using an  $\omega$  closer to  $f_{22}$ . For the particular case shown in Figure 6,  $f_{21}$  and  $f_{22}$  are both determined to within  $\pm 1\%$  by the spectrum for  $\omega = 0.88$ ; but this is not always the case. In general, the accurate evaluation of the eigenfrequencies requires that they be determined in decreasing order.

The damping is obtained after the data is processed by a digital filter. Usually a band pass filter is used with the high and low band pass limits determined by a frequency band around a peak in the  $|F|$  curve. The result of applying a band pass filter with limits (0.11, 0.15) Hz to the data in Figure 5 is shown in Figure 7. The damping  $\alpha_{22}$  is obtained from the logarithmic decay of the maxima and minima in this filtered data.

The filter, however, introduces distortion at the beginning and end of the data range. In some cases only a few maxima and minima are free from distortion so that spurious values of  $\alpha_{kn}$  are obtained if all are used. Discarding all but the few not distorted increases the error in  $\alpha_{kn}$ . This error is a function of  $Re$ ,  $k$ , and  $n$ . The number of undistorted maxima and minima could be increased by judiciously adjusting the parameters of the system.

Another difficulty occurred when the above process was applied to  $Re = 100$  and 200 cases. The damping was so large that accurate values for  $f_{21}$  could not be obtained and a second peak in  $|F|$ , to determine  $f_{22}$ , could not be found. A method of preprocessing the data was developed to overcome this. It will be illustrated for  $k = 2$ ,  $n = 1, 2$ .

It is assumed that the data can be approximated by the form of expansion given in (4) plus a contribution from the noise in the data,  $n(t)$ , arising from the finite difference approximation. Therefore, with obvious changes in notation in (4), the  $\Delta p_1$  data can be expressed as

$$\Delta p_1 = a_1 e^{-\alpha_{21} t} \sin f_{21} t + a_2 e^{-\alpha_{22} t} \sin f_{22} t + \dots + n(t)$$



where  $\bar{t} = t - t_c$  and  $a_i$  are related to  $A_i$  and the other constants. Let  $\bar{\alpha}_{21}$  be a first approximation to the unknown  $\alpha_{21}$  such that  $\bar{\alpha}_{21} < \alpha_{21}$ ; if the inequality is not satisfied, this will be apparent in the preprocessed data.

The  $\Delta p_1$  data is modified by multiplying it by  $e^{\bar{\alpha}_{21}\bar{t}}$ . Thus, a new time series is generated, giving the preprocessed data:

$$e^{\bar{\alpha}_{21}\bar{t}} \Delta p_1 = a_1 e^{-(\alpha_{21} - \bar{\alpha}_{21})\bar{t}} \sin f_{21}\bar{t} + a_2 e^{-(\alpha_{22} - \bar{\alpha}_{21})\bar{t}} \sin f_{22}\bar{t} + \dots + e^{\bar{\alpha}_{21}\bar{t}} n(t) \quad (7)$$

The noise is negligible except near the end of the record where  $\Delta p_1$  is small. Since  $n(t)$  is not an exponentially damped function, the last term in (7) is amplified and diverges for increasing  $\bar{t}$ . However, this does not prevent the determination of  $f_{21}$  and  $f_{22}$  from the Fourier transform of the preprocessed data because the eigenfrequencies are less than 1 Hz, whereas the noise contributes to higher frequencies, typically 2 Hz and greater. From (7), the effective damping is reduced, enabling  $f_{21}$  and  $f_{22}$  to be determined if  $\bar{\alpha}_{21} < \alpha_{21}$ . The data will diverge for  $\bar{t} > 0$  if  $\bar{\alpha}_{21} > \alpha_{21}$ . In that case  $\bar{\alpha}_{21}$  must be decreased and the process repeated. It is feasible to try several values of  $\bar{\alpha}_{21}$  since obtaining the preprocessed data is simple and inexpensive. The preprocessed data are treated as before to yield  $\alpha_{21} - \bar{\alpha}_{21}$  and  $\alpha_{22} - \bar{\alpha}_{21}$ .

An example of the result of preprocessing is shown in Figure 8. The  $\Delta p_1$  data, for  $Re = 100$ , are in the form of a highly damped sine wave. The Fourier transform of this data, shown in Figure 8a, has only one peak at  $\nu_f = 0.177$  Hz, corresponding to  $f_{21}$ . The transform of the preprocessed data with  $\bar{\alpha}_{21} = 0.30$ , shown in Figure 8b, has two peaks. The peak at the higher frequency has shifted to  $\nu_f = 0.189$  Hz, which is a more accurate value for  $f_{21}$  than 0.177 Hz. The peak at the lower frequency occurs at  $\nu_f = 0.089$  Hz, giving  $f_{22}$ . Values for  $f_{21}$  and  $f_{22}$  to within 3% of the above values are obtained with  $\bar{\alpha}_{21} = 0.36$ . These two values of  $\bar{\alpha}_{21}$  can be compared with  $\alpha_{21} = 0.40$ , the value finally determined. Preprocessing thus enables the  $f_{kn}$  and  $\alpha_{kn}$  to be determined for  $Re = 100$  and 200; however, their accuracy is less than that for higher  $Re$ .

## V. RESULTS

The  $f_{kn}$  and  $\alpha_{kn}$  were determined by the procedures described in Section IV for  $10^2 \leq Re \leq 5 \times 10^4$ ,  $c/a = 1$ ,  $n = 1, 2, 3$ , and  $k = 2, 4$ . Some points in this parameter space are not included here. These results are compared with the  $C_R$  and  $C_I$  obtained from the linear theory.

In Figure 9 the  $f_{2n}$  are compared with the eigenfrequencies  $C_{R_{2n}}$ . For  $Re = 10^3$  and  $n = 1, 2$  the  $f_{2n}$  and  $C_{R_{2n}}$  are both essentially the same as the values calculated for inviscid flow; however, significant difference is found for  $f_{23}$  at  $Re = 10^3$ .

For  $Re < 10^3$  the differences between  $f_{2n}$  and  $C_{R_{2n}}$  increase. The results for  $Re = 100, 200$  are shown by bars indicating the variation obtained as the various parameters of the analysis process are changed; for the other symbols the variation is  $\pm 1\%$ . The  $f_{22}$  appear to be nonmonotonic at the lower  $Re$ . The  $C_{R_{2n}}$  are nonmonotonic to a slight degree. In the application of the calculated frequencies to the liquid-filled projectile, an accuracy of a few per cent is required.

In Figure 10 the  $\alpha_{2n}$  are compared with  $C_{I_{2n}}$ . They agree to within  $\pm 5\%$  for  $Re > 10^3$ , but the deviations are considerably more for lower  $Re$ , the largest being for  $\alpha_{22}$  at  $Re = 100$ ;  $\alpha_{22}$  is definitely nonmonotonic. For  $n = 1$  the result from the theory of Kudlick<sup>9</sup> is also shown. This theory uses a matched-asymptotic expansion in powers of  $Re^{-1/2}$ , but only the lowest term in  $Re^{-1/2}$  is calculated. The straight line from Kudlick's theory falls into the curve for  $C_{I_{21}}$  at about  $Re = 10^5$ , but it deviates increasingly for  $Re < 10^5$ . If the curve of  $C_I$  vs  $Re$  for  $n = 1$ , from the linear theory, is fitted to powers of  $Re$ , starting from  $Re^{-1/2}$ , the next term is found to be  $Re^{-1.04}$ , indicating that the next term in Kudlick's expansion is necessary to obtain a result which agrees with those from the numerical simulation. The presence of  $\log Re$  in the expansion might not be detected from this curve fit.

The same type of results, for frequency and damping vs  $Re$ , are shown in Figures 11 and 12, respectively, for  $k = 4$ . For  $Re = 10^3$ ,  $f_{4n} - C_{R_{4n}}$  are slightly larger than for the  $k = 2$  case whereas  $\alpha_{4n} - C_{I_{4n}}$  are negligible, as for  $k = 2$ . The differences between the results of the Kudlick theory and those of either the linear eigenvalue theory or the numerical simulation are greater for the  $k = 4$  case than those shown in Figure 10 for  $k = 2$ .

## VI. CONCLUSIONS

By means of a numerical simulation, the results of a linear eigenvalue theory with correction have been validated. Although no results without the correction were discussed, the calculations showed that errors of several percent in  $C_R$  and up to a factor of 2 in  $C_I$  are obtained if the correction is not applied. With correction, the predicted  $C_R$  agree with the  $f$  to within  $\pm 2\%$  for the  $k = 2$  mode and 3.5% for the  $k = 4$  mode; the  $C_I$  agree with the  $\alpha$  to within  $\pm 2\%$  for the  $k = 2$  mode and 6.5% for the  $k = 4$  mode, for  $Re > 10^3$ . For  $Re < 10^3$  extraction of  $f$  and  $\alpha$  from the pressure data, using Fourier transform and digital filter techniques, becomes more difficult, and the uncertainty in the results increases.

## ACKNOWLEDGMENTS

The authors are indebted to Mr. William Mermagen for providing them with the Fourier transform and digital filter programs and his aid in related parts of this work. They also thank Dr. Paul Neitzel for his contributions to the graphics programs.

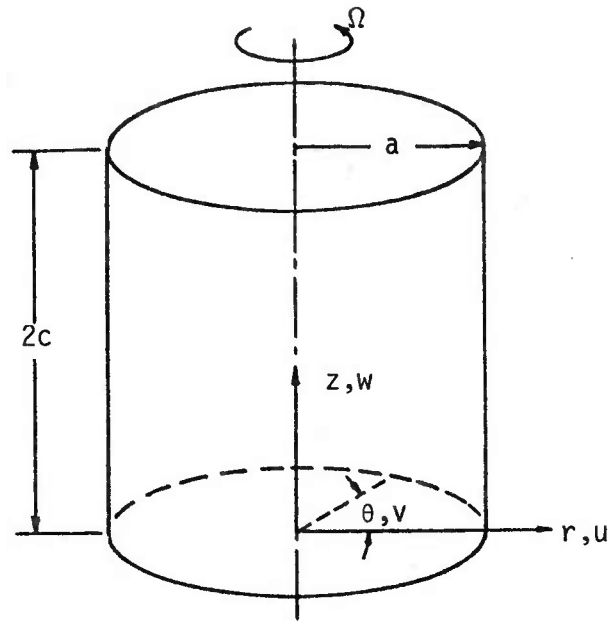


Figure 1. Cylinder, Coordinates, and Notation

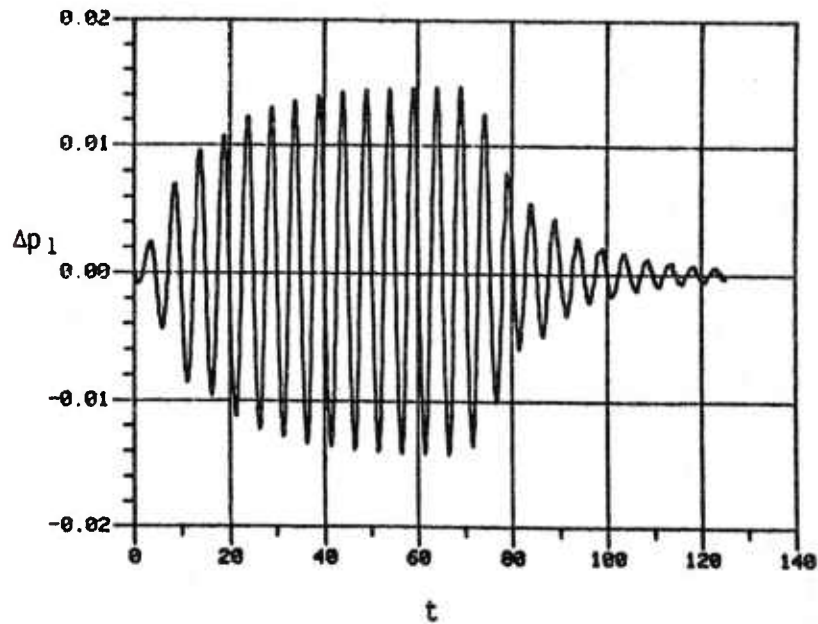


Figure 2. Typical Pressure History -  $\Delta p_1$  vs  $t$  for Perturbed Solid Body Rotation with Single Mode Excitation ( $Re = 1.0 \times 10^3$ ,  $c/a = 1.0$ ,  $\varepsilon = 0.05$ ,  $\omega = 1.15$ ,  $t_c = 70.375$ ).

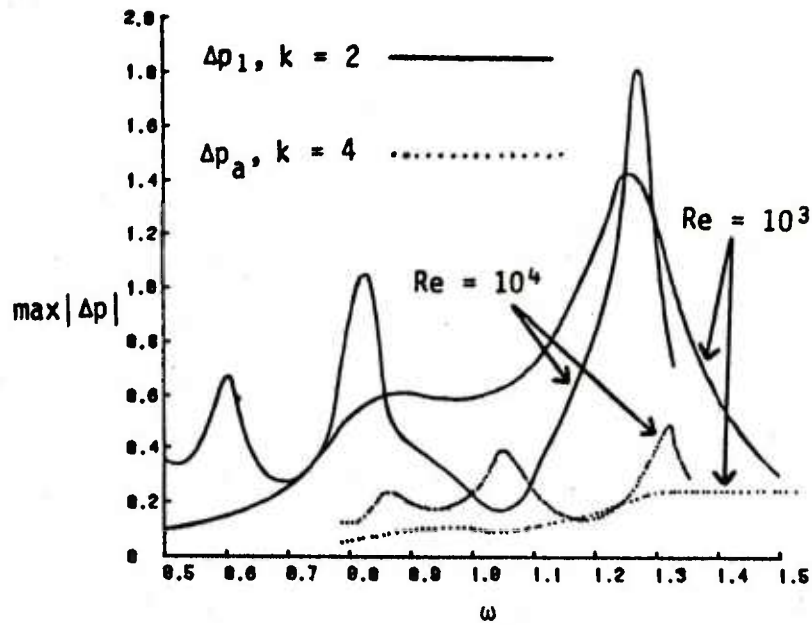


Figure 3. Amplitude Response Curve -  $\max |\Delta p|$  vs Forcing Frequency ( $c/a = 1.0$ ,  $\varepsilon = 0.05$ ).

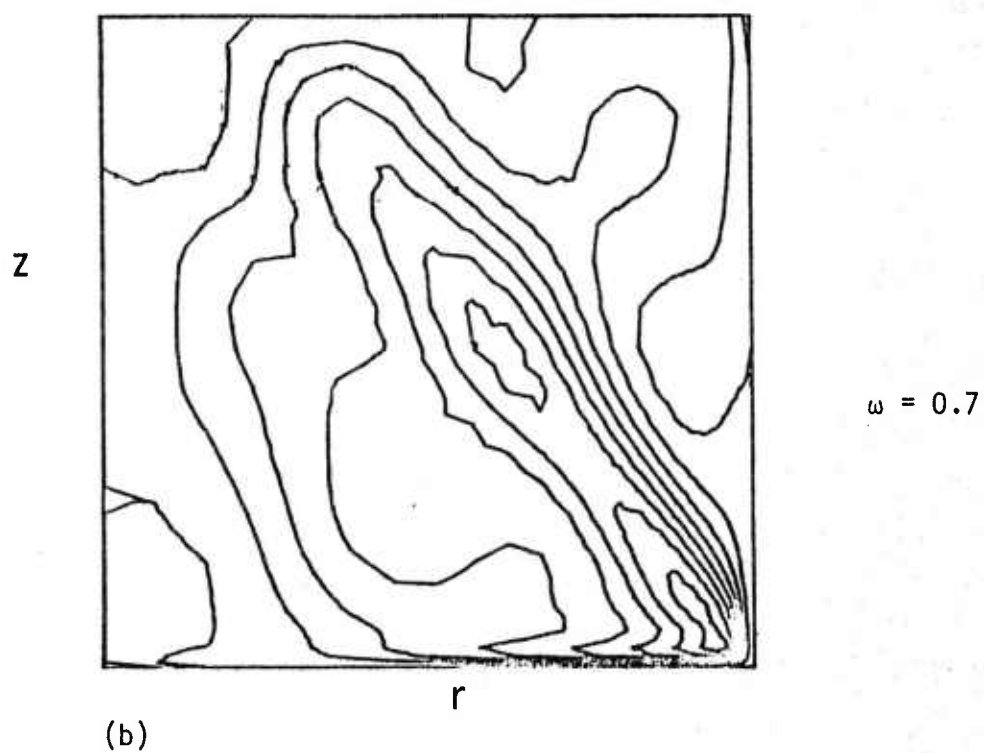
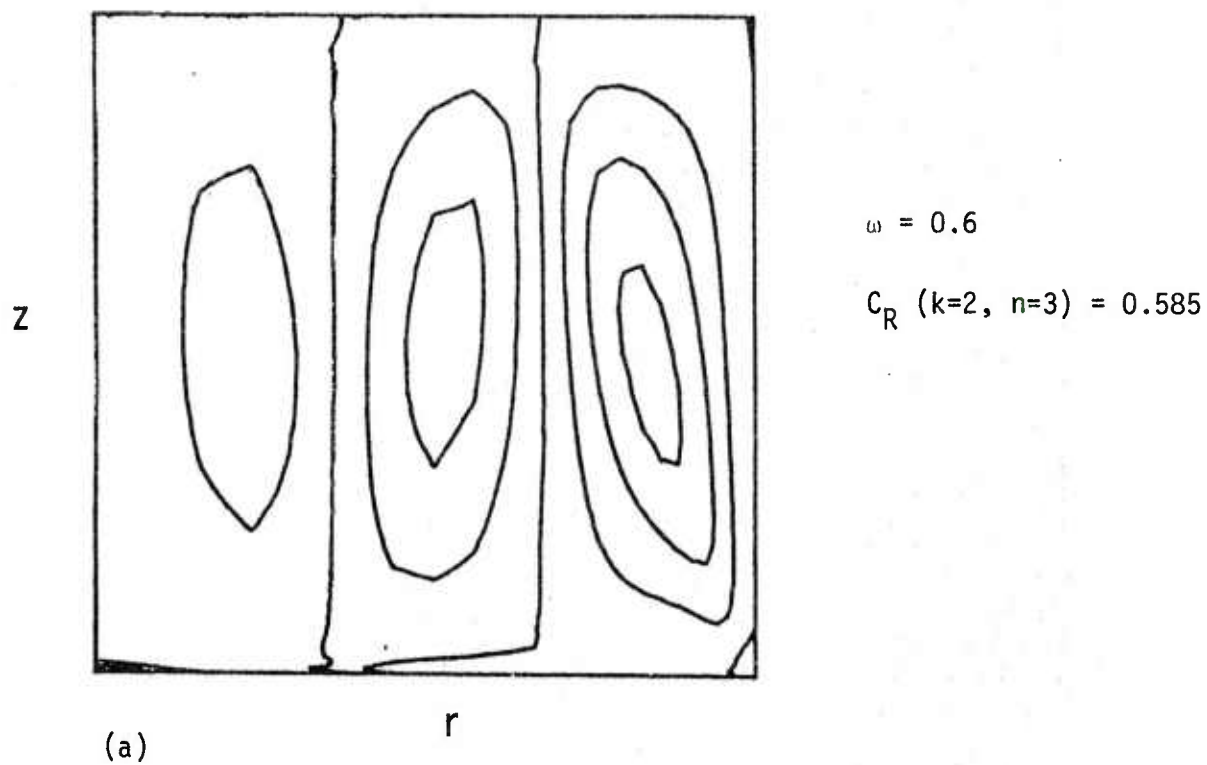
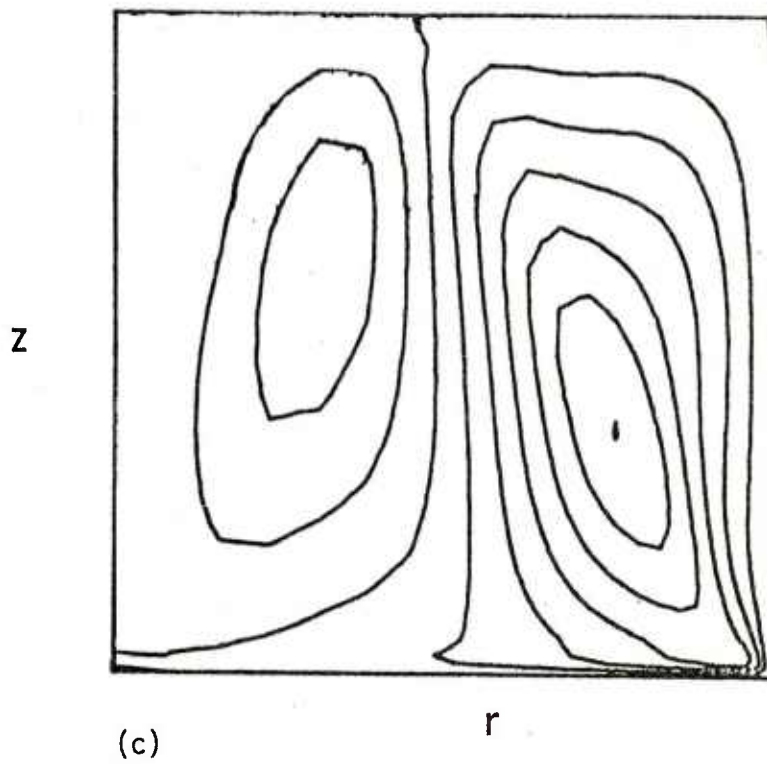
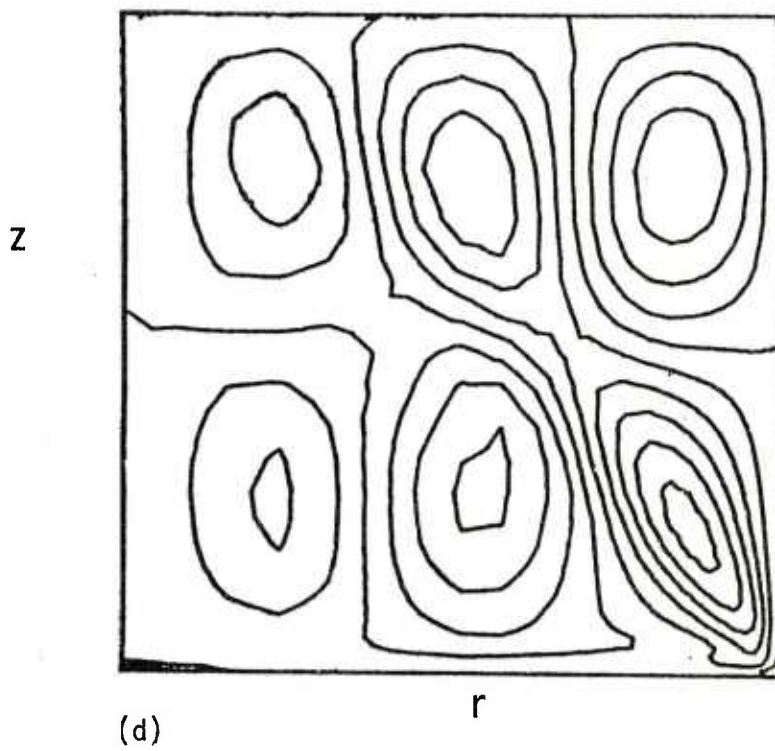


Figure 4. Instantaneous Meridional Streamlines for Four Perturbation Frequencies ( $Re = 1 \times 10^4$ ,  $c/a = 1.0$ ,  $\epsilon = 0.05$ ).



$$\omega = 0.8$$

$$C_R (k=2, n=2) = 0.812$$



$$\omega = 1.05$$

$$C_R (k=4, n=3) = 1.05$$

Figure 4. Instantaneous Meridional Streamlines for Four Perturbation Frequencies ( $Re = 1 \times 10^4$ ,  $c/a = 1.0$ ,  $\epsilon = 0.05$ ) (continued).



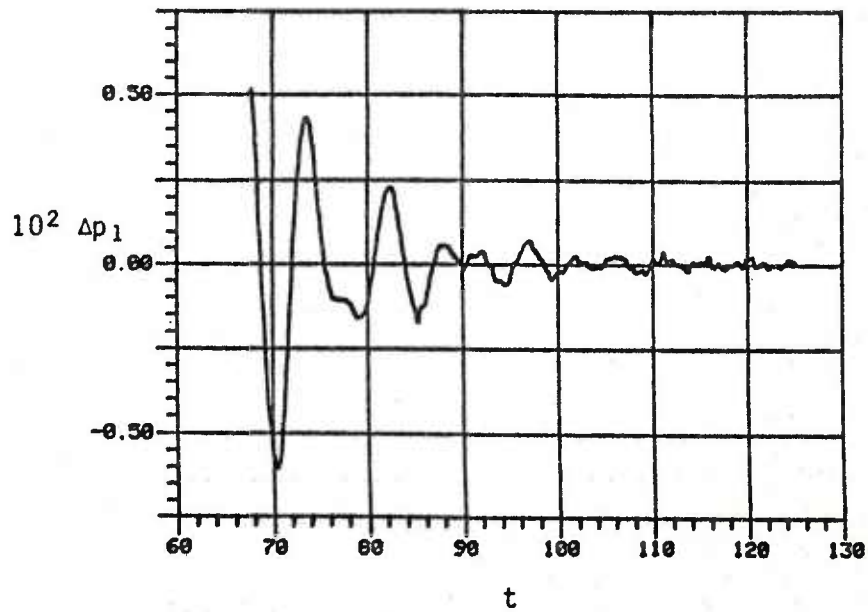


Figure 5. Pressure History,  $\Delta p_1$  After Cut-Off for a Case With Two Dominant Modes ( $Re = 1.0 \times 10^3$ ,  $c/a = 1.0$ ,  $\epsilon = 0.05$ ,  $\omega = 0.88$ ,  $t_c = 67.875$ ).

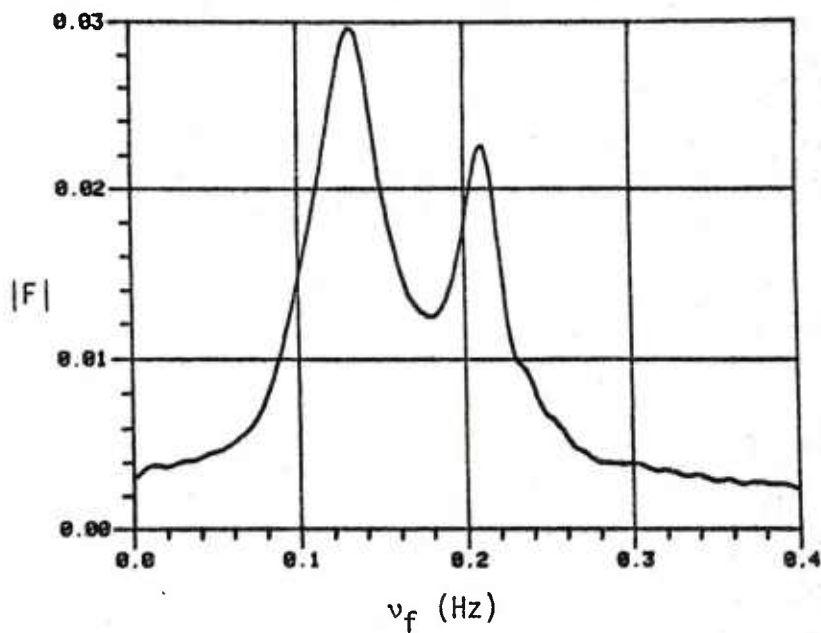


Figure 6. Fourier Transform of the Pressure History Shown in Figure 5 ( $Re = 1.0 \times 10^3$ ,  $c/a = 1.0$ ,  $\epsilon = 0.05$ ).

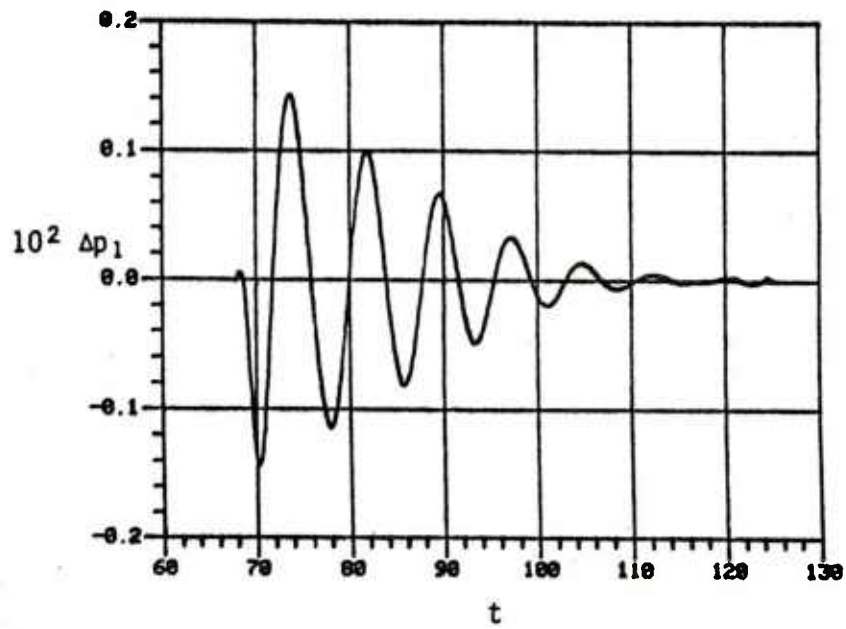


Figure 7. Band Pass Filter of the Pressure History  
 Shown in Figure 5 ( $Re = 1.0 \times 10^3$ ,  $c/a = 1.0$ ,  $\epsilon = 0.05$ ,  $t_c = 67.875$ ,  $0.11 \leq v_f \leq 0.15$ ).

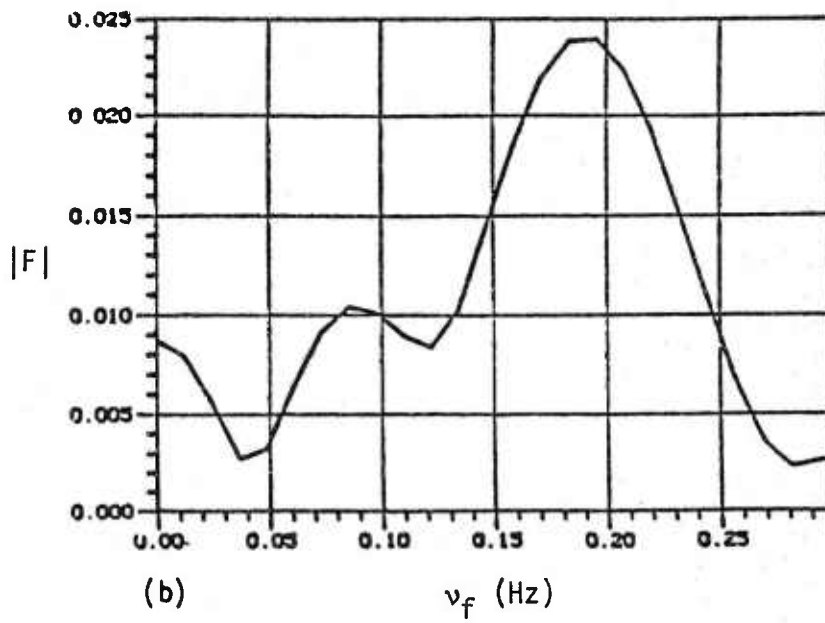
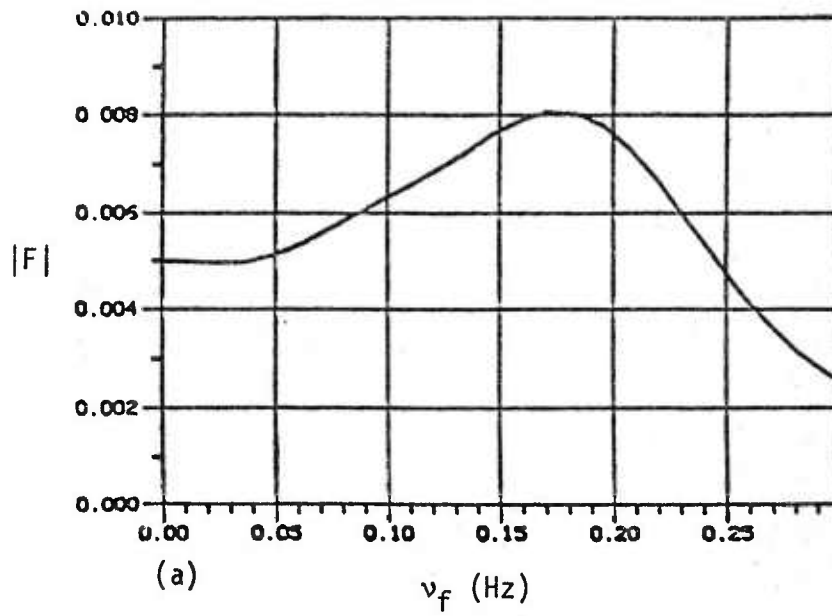


Figure 8. Comparison of Fourier Transforms (a) Before and (b) After Preprocessing the Data ( $Re = 100.0$ ,  $c/a = 1.0$ ,  $\epsilon = 0.05$ ,  $\omega = 0.83$ ,  $t_c = 40.0$ ,  $40.0 \leq t \leq 53.0$ ,  $\bar{\alpha}_{21} = 0.3$ ).

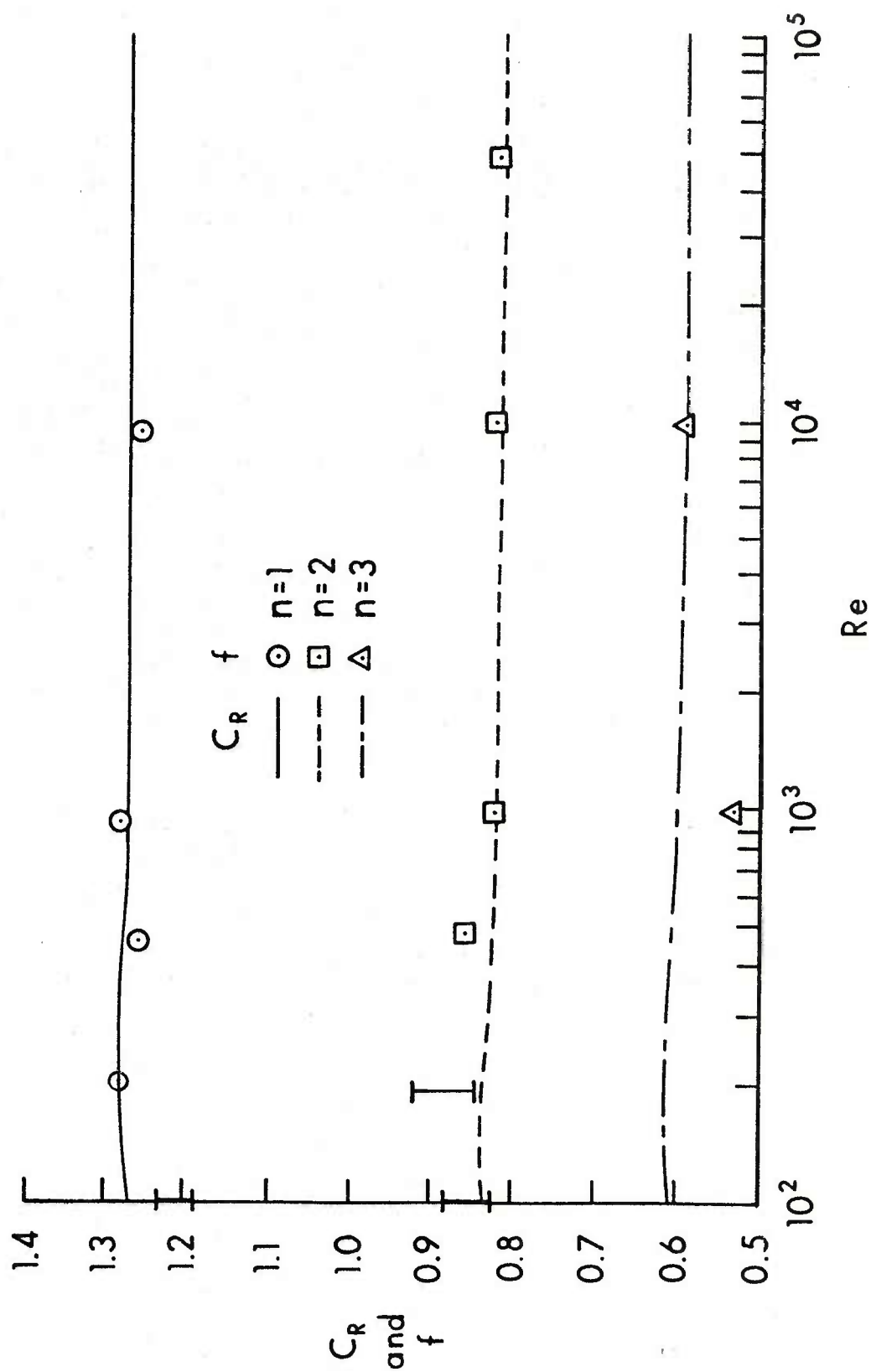


Figure 9. Comparison of Eigenfrequencies From Linear Theory With Correction,  $C_R$ , and Those From Numerical Simulation,  $f$  ( $c/a = 1.0$ ,  $k = 2$ ).

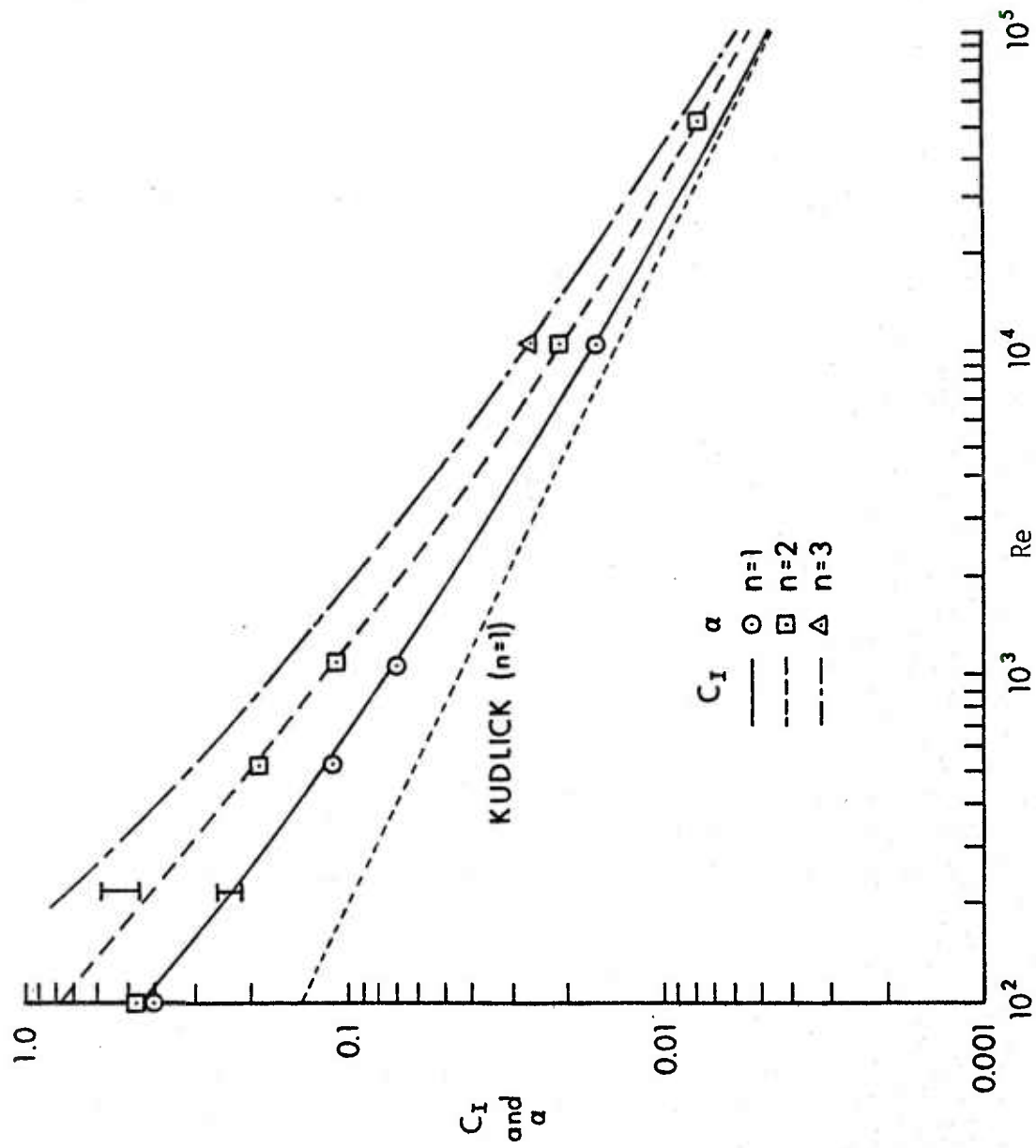


Figure 10. Comparison of Wave Dampings From Linear Theory,  $C_I$ , With Those From Numerical Simulation,  $\alpha$ , and From Kudlick Theory ( $c/a = 1.0$ ,  $k = 2$ ).

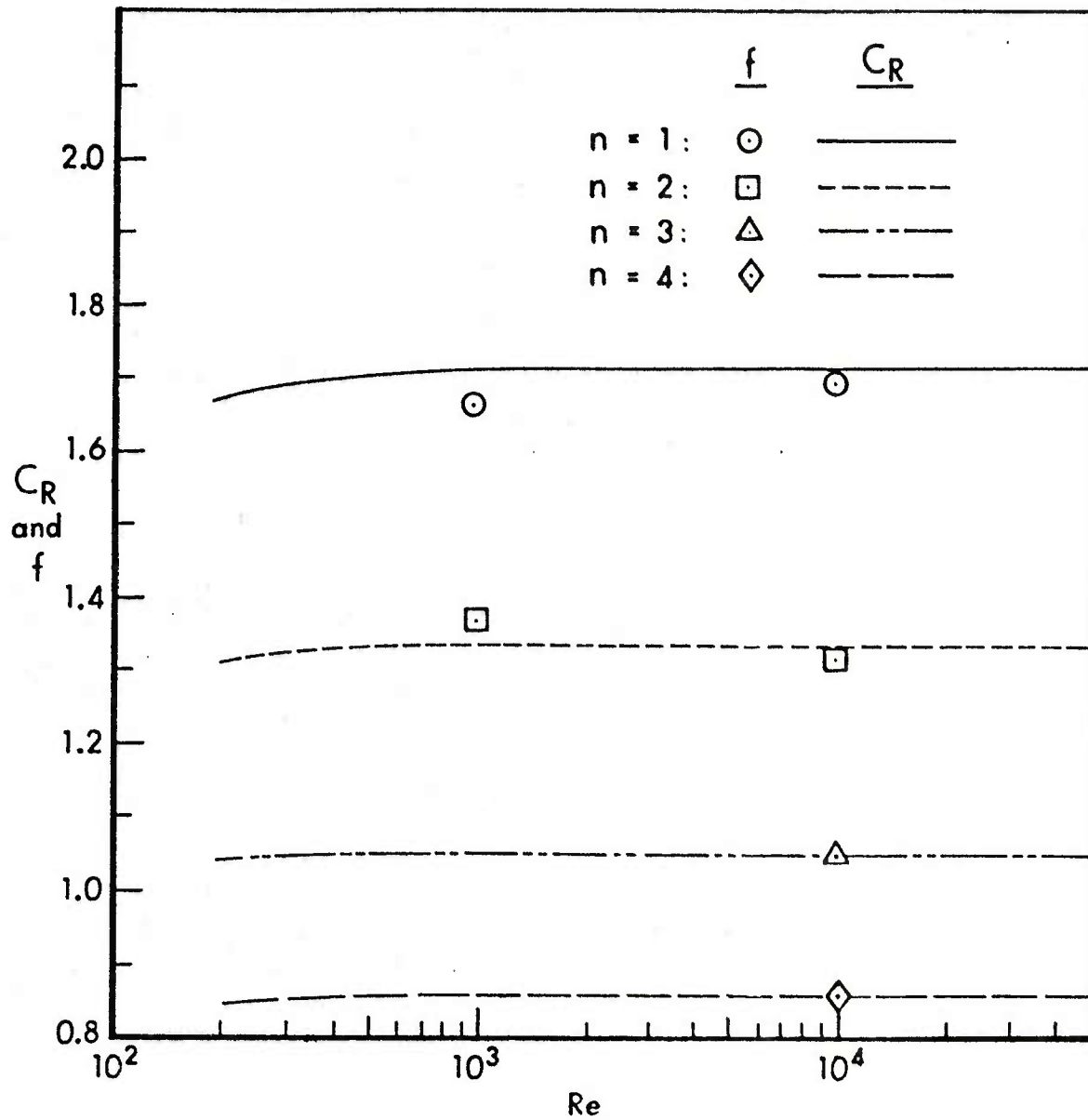


Figure 11. Comparison of Eigenfrequencies From Linear Theory With Correction,  $C_R$ , and Those From Numerical Simulation,  $f$  ( $c/a = 1.0$ ,  $k = 4$ ).

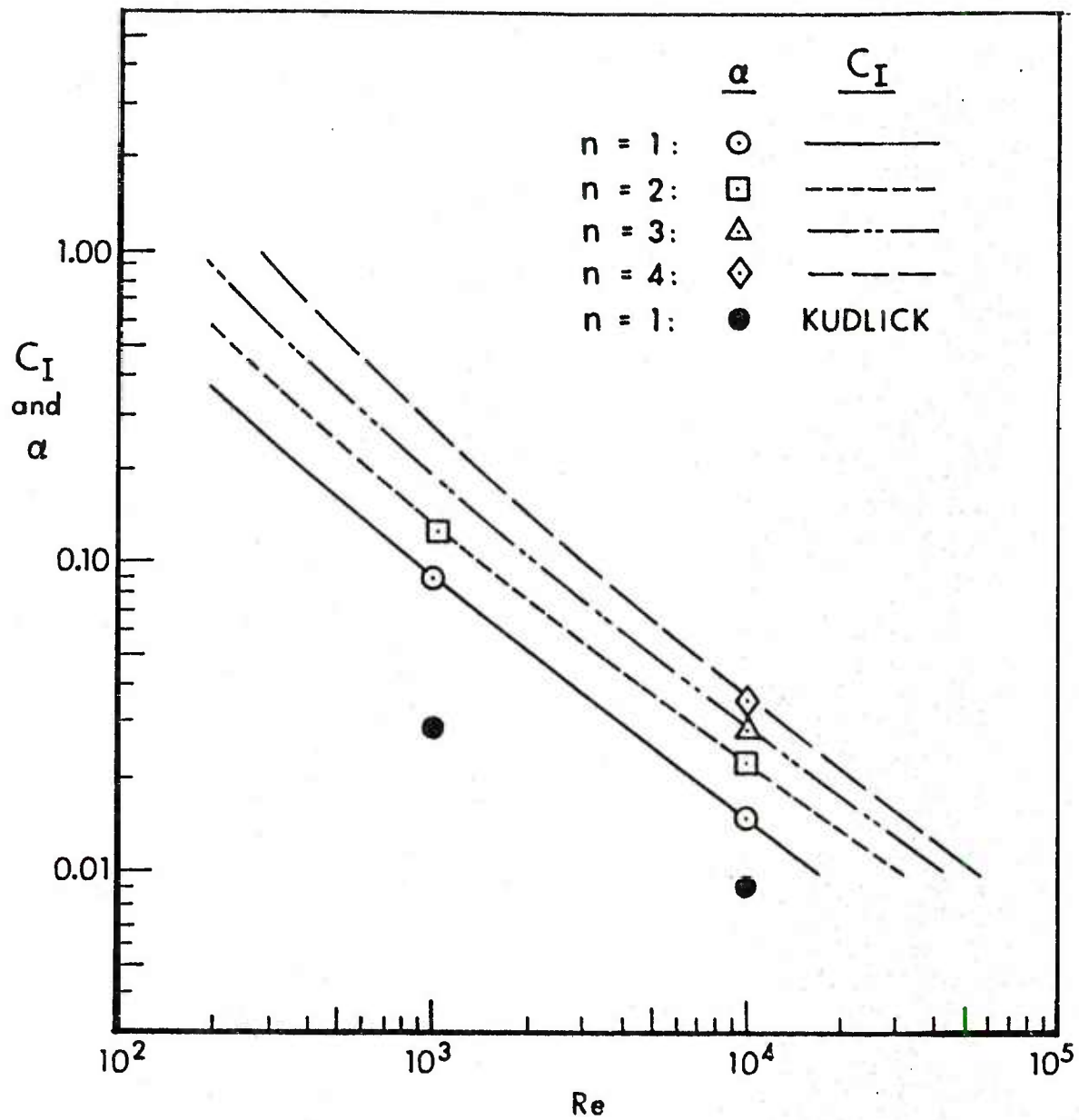


Figure 12. Comparison of Wave Dampings From Linear Theory,  $C_I$ , With Those From Numerical Simulation,  $\alpha$ , and From Kudlick Theory ( $c/a = 1.0$ ,  $k = 4$ ).



## REFERENCES

1. K. Stewartson, "On the Stability of a Spinning Top Containing Liquid," J. Fluid Mech., Vol. 5, Part 4, September 1959, pp. 577-592.
2. E. H. Wedemeyer, "Viscous Corrections to Stewartson's Stability Criterion," BRL Report No. 1325, Aberdeen Proving Ground, Maryland, June 1966 (AD 489687). Also "Dynamics of Liquid-Filled Shell: Theory of Viscous Corrections to Stewartson's Stability Problem," BRL Report No. 1287, June 1965 (AD 472474).
3. C. W. Kitchens, Jr., N. Gerber, and R. Sedney, "Oscillations of a Liquid in a Rotating Cylinder: Part I. Solid Body Rotation," Technical Report ARBRL-TR-02081, June 1978 (AD A057759).
4. R. D. Whiting and N. Gerber, "Dynamics of a Liquid-Filled Gyroscope: Update of Theory and Experiment," Technical Report ARBRL-TR-02221, March 1980 (AD A083886).
5. C. W. Kitchens, Jr., "Navier-Stokes Solutions for Spin-Up in a Filled Cylinder," AIAA Journal, Vol. 18, No. 8, August 1980, pp. 929-934. Also Technical Report ARBRL-TR-02193, September 1979 (AD A077115).
6. K. D. Aldridge, "Experimental Verification of the Inertial Oscillations of a Fluid in a Cylinder During Spin-Up," BRL Contract Report No. 273, Aberdeen Proving Ground, Maryland, September 1975 (AD A018797). Also Geophys. Astrophys. Fluid Dynamics, Vol. 8, 1977, pp. 279-301.
7. K. D. Aldridge and S. Stergiopoulos, "Recovery of Complex Eigenfrequencies of Inertial Waves by Linearized Inversion of Viscous Decay Records," to be submitted for publication. See also S. Stergiopoulos, "An Experimental Study of Inertial Waves in a Fluid Contained in a Rotating Cylindrical Cavity During Spin-Up From Rest," Ph.D Thesis, York University, Toronto, Ontario, February 1982.
8. D. Fultz, "A Note on Overstability and the Elastoid-Inertia Oscillations of Kelvin, Solberg, and Bjerkness," J. Meteorology, Vol. 16, April 1959, pp. 199-208.
9. M. D. Kudlick, "On the Transient Motion of a Contained Rotating Fluid," Ph.D Thesis, Massachusetts Institute of Technology, 1966.
10. H. P. Greenspan, The Theory of Rotating Fluids, Cambridge University Press, New York, NY, 1968, pp. 81ff.

## APPENDIX A

### Determination of Pressure from Stream Function

## APPENDIX: DETERMINATION OF PRESSURE FROM STREAM FUNCTION

The nondimensional Navier-Stokes axial momentum equation (e. g., (3.33c) of Reference A-1) for incompressible axisymmetric flow is integrated with respect to  $z$  at  $r = 0$ :

$$p(0,z,t) - p(0,0,t) = \int_0^z \left\{ (1/\text{Re}) [w_{rr} + (1/r) w_r + w_{zz}] - [w_t + w w_z] \right\} dz, \quad (\text{A.1})$$

where subscripts denote partial derivatives. Kitchens<sup>5</sup> did not calculate  $w$ , but rather the stream function  $\psi$ . By definition

$$w = - \psi_r / r. \quad (\text{A.2})$$

This shows how  $p$  is obtained, in principle. Its evaluation from the finite difference solution is outlined next. It is inferred from the equations and boundary conditions in Reference 5 that  $\psi$  is an even function of  $r$  and  $\psi(r=0) = 0$ . Then  $\psi$  is expanded in the following form near the axis:

$$\psi(r,z,t) = a_2(z,t)r^2 + a_4(z,t)r^4 + \dots \quad (\text{A.3})$$

It follows from (A.2) that

$$w(r,z,t) = -2 a_2(z,t) - 4 a_4(z,t)r^2 + \dots \quad (\text{A.4})$$

Evaluating the terms on the right-hand side of (A.1) at  $r = 0$  by means of (A.4), we obtain

$$\begin{aligned} p(0,z,t) - p(0,0,t) = & -2[a_2(z,t)]^2 + 2 \frac{\partial}{\partial t} \int_0^z a_2(\xi,t) d\xi - \\ & (16/\text{Re}) \int_0^z a_4(\xi,t) d\xi - \\ & (2/\text{Re}) [(\partial a_2 / \partial z)_{z=z} - (\partial a_2 / \partial z)_{z=0}]. \end{aligned} \quad (\text{A.5})$$

---

A-1. H. Schlichting, Boundary Layer Theory, McGraw-Hill Book Co., New York, NY, 1960.

The functions  $a_2(z,t)$  and  $a_4(z,t)$  are obtained from the finite-difference solution<sup>5</sup> at those values of  $z$  at which  $\psi(r,z,t)$  is computed. A grid point in the finite-difference solution is denoted by  $r_j, z_\ell$ , and the corresponding stream function by  $\psi_{j\ell}$ ;  $j = 1$  for  $r = 0$ , and  $\ell = 1$  for  $z = 0$ . The coefficients  $a_2$  and  $a_4$ , evaluated at  $z = z_\ell$ , are denoted by  $a_{2\ell}$  and  $a_{4\ell}$ , respectively. If we retain only two terms in the expansion (A.3), then in terms of  $\psi_{2\ell}$  and  $\psi_{3\ell}$ :

$$a_{2\ell} \cong [(r_3/r_2)^2 \psi_{2\ell} - (r_2/r_3)^2 \psi_{3\ell}] / [r_3^2 - r_2^2] \quad (A.6)$$

$$a_{4\ell} \cong [-(1/r_2)^2 \psi_{2\ell} + (1/r_3)^2 \psi_{3\ell}] / [r_3^2 - r_2^2].$$

Although the  $a_1$  and  $a_2$  are evaluated only at  $z_\ell$ , they are continuous functions of  $z$ , and the integrals in (A.5) are approximated by numerical integration employing the values of  $a_{2\ell}$  and  $a_{4\ell}$ . Trapezoidal integration is used for  $z = z_2$  and Simpson integration is employed for  $z > z_2$ . For  $a_2$ , e.g., the integral is

$$I_\ell \equiv \int_0^{z_\ell} a_2 dz = \int_0^{\eta_\ell} a_2 (dz/d\eta) d\eta,$$

where  $\eta(z)$  and  $dz/d\eta$  are obtained from the stretching transformation of (17) in Reference 5. Then

$$I_\ell \cong I_{\ell-2} + (\Delta\eta/6) [(a_2)_{\ell-2} (dz/d\eta)_{\ell-2} + 4 (a_2)_{\ell-1} (dz/d\eta)_{\ell-1} + a_{2\ell} (dz/d\eta)_\ell], \quad (A.7)$$

where  $\Delta\eta$  is the constant interval.

The  $\partial a_2 / \partial z$  terms are obtained from the expression

$$a_2(z) \cong a_{2\ell} + C_1 (z - z_\ell) + C_2 (z - z_\ell)^2. \quad (A.8)$$

Then

$$\left( \frac{\partial a_2}{\partial z} \right)_{z=z_\ell} = C_1 = \frac{[(a_2)_a - (a_2)_\ell] (z_b - z_\ell)^2 - [(a_2)_b - (a_2)_\ell] (z_a - z_\ell)^2}{(z_a - z_\ell) (z_b - z_\ell) (z_b - z_a)}, \quad (A.9)$$

where  $z_a$  and  $z_b$  are grid points either adjacent to  $z_\ell$  or one point removed. Finally, the time derivative of a function,  $g$ , beginning at  $t = 2\Delta t$  is approximated by

$$(dg/dt)_{t=t_i} = [3 g_i - 4 g_{i-1} + g_{i-2}]/(2\Delta t), \quad (\text{A.10})$$

where  $\Delta t$  is the constant time interval of the calculation.

# LIST OF SYMBOLS

$a$	cross-sectional radius of cylinder
$A_{kn}$	coefficient of $kn$ term in $z,t$ expansion of $p(0,z,t)$ in (3)
$c$	half-height of cylinder/ $a$
$C$	$\equiv C_R + i C_I$ , complex eigenfrequency of rotating fluid
$C_I$	decay rate/ $\Omega_0$ of inertial oscillation computed by linear theory
$C_R$	frequency/ $\Omega_0$ of inertial oscillation computed by linear theory
$f_{kn}$	frequency/ $\Omega_0$ of inertial oscillation determined by numerical simulation
$ F $	magnitude of Fourier transform of pressure history data
$j$	index in $r$ -direction of grid point in finite-difference solution
$k$	axial wave number ((1a) - (1d))
$K$	$\equiv k\pi/(2c)$
$K_C$	$\equiv (k\pi/2)/(c-\delta)$
$\ell$	index in $z$ -direction of grid point in finite-difference solution
$m$	azimuthal wave number (see (1a) - (1d))
$n$	radial wave number
$p$	$\equiv P + \bar{p}^*$ , total pressure/ $(\rho a^2 \Omega_0^2)$
$\bar{p}^*$	perturbation pressure/ $(\rho a^2 \Omega_0^2)$
$\hat{\bar{p}}$	radial variation of $\bar{p}^*$ (see (1d))
$P$	unperturbed pressure/ $(\rho a^2 \Omega_0^2)$
$r$	radial coordinate
$Re$	$\equiv \Omega_0 a^2/\nu$ , Reynolds number
$t$	time $\times \Omega_0$
$t_c$	cutoff time $\times \Omega_0$ of perturbation on angular velocity of cylinder
$\bar{t}$	$\equiv t - t_c$

$u, v, w$	flow velocities/( $a \Omega_0$ ) in radial, azimuthal, and axial directions, respectively
$u^*, v^*, w^*$	flow perturbation velocities/( $a \Omega_0$ ) in $r, \theta$ , and $z$ directions, respectively
$\hat{u}, \hat{v}, \hat{w}$	radial variation of $u, v, w$ ((1a) - (1c))
$U, V, W$	unperturbed flow velocities/( $a \Omega_0$ ) in $r, \theta$ , and $z$ directions, respectively
$z$	axial coordinate ( $z = 0$ at base of cylinder)
$\alpha_{kn}$	decay rate/ $\Omega_0$ of $k, n$ mode determined by numerical simulation
$\bar{\alpha}_{kn}$	damping factor used in preprocessing data ((7))
$\delta c$	complex boundary layer thickness occurring in the viscous endwall correction to the eigenvalue solution
$\Delta p_a$	$\equiv 0.5 \Delta p_1 - \Delta p_{1/2}$
$\Delta p_1$	$\equiv p(0, c, t) - p(0, 0, t)$
$\Delta p_{1/2}$	$\equiv p(0, c/2, t) - p(0, 0, t)$
$\Delta t$	time interval
$\epsilon$	amplitude of perturbation to angular velocity of cylinder
$\theta$	azimuthal cylindrical coordinate
$\nu$	kinematic viscosity of liquid
$\nu_f$	frequency in Fourier transform plots [Hz]
$\rho$	density of liquid
$\psi$	stream function in Navier-Stokes spin-up flow calculation ((A.2))
$\omega$	frequency/ $\Omega_0$ of perturbation to cylinder spin
$\omega_m$	value of $\omega$ at which peak occurs on response curve in Figure 3
$\Omega_0$	unperturbed angular velocity of cylinder
$\Omega(t)$	forcing function of perturbation to cylinder spin



# DISTRIBUTION LIST

<u>No. of Copies</u>	<u>Organization</u>	<u>No. of Copies</u>	<u>Organization</u>
12	Administrator Defense Technical Information Center ATTN: DTIC-DDA Cameron Station Alexandria, VA 22314	1	Commander US Army Armament Materiel Readiness Command ATTN: DRSAR-LEP-L Rock Island, IL 61299
1	Commander US Army Engineer Waterways Experiment Station ATTN: R.H. Malter P.O. Box 631 Vicksbury, MS 39181	1	Director US Army ARRADCOM Benet Weapons Laboratory ATTN: DRDAR-LCB-TL Watervliet, NY 12189
1	Commander US Army Materiel Development and Readiness Command ATTN: DRCDMD-ST 5001 Eisenhower Avenue Alexandria, VA 22333	1	Commander US Army Aviation Research and Development Command ATTN: DRDAV-E 4300 Goodfellow Blvd St. Louis, MO 63120
1	Commander US Army Armament Research and Development Command ATTN: DRDAR-TDC Dover, NJ 07801	1	Director US Army Air Mobility Research and Development Laboratory ATTN: SAVDL-D, W.J. McCroskey Ames Research Center Moffett Field, CA 94035
3	Commander US Army Armament Research and Development Command ATTN: DRDAR-TSS DRDAR-LC, Dr. J. Frasier Dover, NJ 07801	1	Commander US Army Communications Research and Development Command ATTN: DRSEL-ATDD Fort Monmouth, NJ 07703
6	Commander US Army Armament Research and Development Command ATTN: DRDAR-LCA-F Mr. D. Mertz Mr. E. Falkowski Mr. A. Loeb Mr. R. Kline Mr. S. Kahn Mr. S. Wasserman Dover, NJ 07801	1	Commander US Army Electronics Research and Development Command Technical Support Activity ATTN: DELSD-L Fort Monmouth, NJ 07703
1	Director US Army Air Mobility Research and Development Laboratory Ames Research Center Moffett Field, CA 94035	1	Commander US Army Missile Command ATTN: DRSMI-R Redstone Arsenal, AL 35898
		1	Commander US Army Missile Command ATTN: DRSMI-YDL Redstone Arsenal, AL 35898

# DISTRIBUTION LIST

<u>No. of Copies</u>	<u>Organization</u>	<u>No. of Copies</u>	<u>Organization</u>
1	Commander US Army Missile Command ATTN: DRSMI-RDK, Mr. R. Deep Restone Arsenal, AL 35898	2	Commander David W. Taylor Naval Ship Research & Development Cmd ATTN: H.J. Lugt, Code 1802 S. de los Santos Bethesda, MD 20084
1	Commander US Army Tank Automotive Command ATTN: DRSTA-TSL Warren, MI 48090	1	Commander Naval Surface Weapons Center ATTN: DX-21, Lib Rr Dahlgren, VA 22448
1	Commander US Army Jefferson Proving GD ATTN: STEJP-TD-D Madison, IN 47251	4	Commander Naval Surface Weapons Center Applied Aerodynamics Division ATTN: K.R. Enkenhus M. Ciment A.E. Winklemann W.C. Ragsdale Silver Spring, MD 20910
2	Commander US Army Research Office ATTN: Dr. R.E. Singleton Dr. Jagdish Chandra P.O. Box 12211 Research Triangle Park, NC 27709	1	AFATL (DLDL, Dr. D.C. Daniel) Eglin AFB, FL 32542
1	AGARD-NATO ATTN: R.H. Korkegi APO New York 09777	2	AFFDL (W.L. Hankey; J.S. Shang) Wright-Patterson AFB, OH 45433
1	Director US Army TRADOC Systems Analysis Activity ATTN: ATAA-SL White Sands Missile Range NM 88002	5	Director National Aeronautics and Space Administration Ames Research Center ATTN: D.R. Chapman J. Rakich W.C. Rose R. Wick P. Kutler Moffett Field, CA 94035
2	Commandant US Army Infantry School ATTN: ATSH-CD-CSO OR Fort Benning, GA 31905	4	Director National Aeronautics and Space Administration Langley Research Center ATTN: E. Price J. South J.R. Sterrett Tech Library Langley Station Hampton, VA 23365
3	Commander Naval Air Systems Command ATTN: AIR-604 Washington, DC 20360		

# DISTRIBUTION LIST

<u>No. of Copies</u>	<u>Organization</u>	<u>No. of Copies</u>	<u>Organization</u>
1	Aerospace Corporation Aero-Engineering Subdivision ATTN: Walter F. Reddall El Segundo, CA 90245	3	Boeing Commercial Airplane Company ATTN: R.A. Day, MS 1W-82 P.E. Rubbert, MS 3N-19 J.D. McLean, MS-3N-19 Seattle, WA 98124
1	Director National Aeronautics and Space Administration Lewis Research Center ATTN: MS 60-3, Tech Lib 21000 Brookpark Road Cleveland, OH 44135	3	Calspan Corporation ATTN: A. Ritter G. Homicz W. Rae P.O. Box 400 Buffalo, NY 14225
2	Director National Aeronautics and Space Administration Marshall Space Flight Center ATTN: A.R. Felix, Chief S&E-AERO-AE Dr. W.W. Fowles Huntsville, AL 35812	1	General Dynamics ATTN: Research Lib 2246 P.O. Box 748 Fort Worth, TX 76101
2	Director Jet Propulsion Laboratory ATTN: L.M. Mach Tech Library 4800 Oak Grove Drive Pasadena, CA 91103	1	General Electric Company, RESD ATTN: W.J. East 3198 Chestnut Street Philadelphia, PA 19101
3	Arnold Research Org., Inc. ATTN: J.D. Whitfield R.K. Matthews J.C. Adams Arnold AFB, TN 37389	2	Grumman Aerospace Corporation ATTN: R.E. Melnik L.G. Kaufman Bethpage, NY 11714
3	Aerospace Corporation ATTN: H. Mirels R.L. Varwig Aerophysics Lab. P.O. Box 92957 Los Angeles, CA 90009	2	Lockheed-Georgia Company ATTN: B.H. Little, Jr. G.A. Pounds Dept 72074, Zone 403 86 South Cobb Drive Marietta, GA 30062
1	AVCO Systems Division ATTN: B. Reeves 201 Lowell Street Wilmington, MA 01887	1	Lockheed Missiles and Space Company ATTN: Tech Info Center 3251 Hanover Street Palo Alto, CA 94304
		3	Martin-Marietta Laboratories ATTN: S.H. Maslen S.C. Traugott H. Obremski 1450 S. Rolling Road Baltimore, MD 21227

# DISTRIBUTION LIST

<u>No. of Copies</u>	<u>Organization</u>	<u>No. of Copies</u>	<u>Organization</u>
2	McDonnell Douglas Astronautics Corporation ATTN: J. Xerikos H. Tang 5301 Bolsa Avenue Huntington Beach, CA 92647	1	Cornell University Graduate School of Aero Engr ATTN: Library Ithaca, NY 14850
2	McDonnell-Douglas Corporation Douglas Aircraft Company ATTN: T. Cebeci K. Stewartson 3855 Lakewood Boulevard Long Beach, CA 90801	3	California Institute of Technology ATTN: Tech Library H.B. Keller, Math Dept D. Coles, Aero Dept Pasadena, CA 91109
2	Rockwell International Science Center ATTN: Dr. V. Shankar Dr. N. Malmuth 1049 Camino Dos Rios Thousand Oaks, CA 91360	1	Illinois Institute of Tech ATTN: H. M. Nagib 3300 South Federal Chicago, IL 60616
3	Sandia Laboratories ATTN: F.G. Blottner W.L. Oberkamp Tech Lib. Albuquerque, NM 87115	1	The Johns Hopkins University Dept of Mech and Materials Sci. ATTN: S. Corrsin Baltimore, MD 21218
2	United Aircraft Corporation Research Laboratory ATTN: M.J. Werle Library East Hartford, CT 06108	4	Director Johns Hopkins University Applied Physics Laboratory ATTN: Dr. R.D. Whiting Dr. D.A. Hurdif Dr. R.S. Hirsh Mr. E.R. Bohn Johns Hopkins Road Laurel, MD 20707
1	LTV Aerospace Corp. Vought Systems Division ATTN: J.M. Cooksey, Chief, Gas Dynamics Lab, 2-53700 P.O. Box 5907 Dallas, TX 75222	1	Louisiana State Univeristy Dept. of Physics and Astronomy ATTN: Dr. R.G. Hussey Baton Rouge, LA 70803
1	Arizona State University Department of Mechanical and Energy Systems Engineering ATTN: G.P. Neitzel Tempe, AZ 85281	3	Massachusetts Institute of Technology ATTN: E. Covert H. Greenspan Tech Lib 77 Massachusetts Avenue Cambridge, MA 02139

# DISTRIBUTION LIST

<u>No. of Copies</u>	<u>Organization</u>	<u>No. of Copies</u>	<u>Organization</u>
2	North Carolina State Univ Mechanical and Aerospace Engineering Department ATTN: F.F. DeJarnette J.C. Williams Raleigh, NC 27607	1	Rensselaer Polytechnic Institute Department of Math Sciences ATTN: R.C. Diprima Troy, NY 12181
1	Northwestern University Department of Engineering Science and Applied Mathematics ATTN: Dr. S.H. Davis Evanston, IL 60201	1	University of California Davis ATTN: H. A. Dwyer Davis CA 95616
1	Notre Dame University Department of Aero Engr ATTN: T.J. Mueller South Bend, IN 46556	1	San Diego State University Department of Aerospace Engr and Engineering Mechanics College of Engineering ATTN: K.C. Wang San Diego, CA 92115
2	Ohio State University Dept of Aeronautical and Astronautical Engineering ATTN: S.L. Petrie O.R. Burggraf Columbus, OH 43210	1	Southern Methodist University Department of Civil and Mechanical Engineering ATTN: R.L. Simpson Dallas, TX 75222
2	Polytechnic Institute of New York ATTN: G. Moretti S.G. Rubin Route 110 Farmingdale, NY 11735	1	Southwest Research Institute Applied Mechanics Reviews 8500 Culebra Road San Antonio, TX 78228
3	Princeton University James Forrestal Research Ctr Gas Dynamics Laboratory ATTN: S.M. Bogdonoff S.I. Cheng Tech Library Princeton, NJ 08540	2	Stanford University Dept of Aeronautics/Astronautics ATTN: Dr. J.L. Steger Dr. S. Chakravarthy Stanford, CA 94305
1	Purdue University Thermal Science & Prop Ctr ATTN: Tech Library W. Lafayette, IN 47907	1	Texas A&M University College of Engineering ATTN: R.H. Page College Station, TX 77843

# DISTRIBUTION LIST

<u>No. of Copies</u>	<u>Organization</u>	<u>No. of Copies</u>	<u>Organization</u>
1	University of California - Berkeley Department of Aerospace Engineering ATTN: M. Holt Berkeley, CA 94720	2	University of Southern California Department of Aerospace Engineering ATTN: T. Maxworthy P. Weidman Los Angeles, CA 90007
2	University of California - San Diego Department of Aerospace Engineering and Mechanical Engineering Sciences ATTN: P. Libby Tech Library La Jolla, CA 92037	2	University of Michigan Department of Aeronautical Engineering ATTN: W.W. Wilmarth Tech Library East Engineering Building Ann Arbor, MI 48104
1	University of Cincinnati Department of Aerospace Engineering ATTN: R.T. Davis Cincinnati, OH 45221	2	University of Rochester Department of Mechanical and Aerospace Sciences ATTN: R. Gans A. Clark, Jr. Rochester, NY 14627
1	University of Colorado Department of Astro-Geophysics ATTN: E.R. Benton Boulder, CO 80304	1	University of Tennessee Department of Physics ATTN: Prof. W.E. Scott Knoxville, TN 37916
2	University of Maryland ATTN: W. Melnik J.D. Anderson College Park, MD 20742	1	University of Texas Department of Aerospace Engineering ATTN: J.C. Westkaemper Austin, TX 78712
1	University of Maryland - Baltimore County Department of Mathematics ATTN: Dr. Y.M. Lynn 5401 Wilkens Avenue Baltimore, MD 21228	1	University of Virginia Department of Aerospace Engineering & Engineering Physics ATTN: I.D. Jacobson Charlottesville, VA 22904
1	University of Santa Clara Department of Physics ATTN: R. Greeley Santa Clara, CA 95053	1	University of Virginia Research Laboratories for the Engineering Sciences ATTN: Prof. H. G. Wood P.O. Box 3366 University Station Charlottesville, VA 22901



# DISTRIBUTION LIST

<u>No. of Copies</u>	<u>Organization</u>	<u>No. of Copies</u>	<u>Organization</u>
1	University of Washington Department of Mechanical Engineering ATTN: Tech Library Seattle, WA 98105		<u>Aberdeen Proving Ground</u>  Director, USAMSAA ATTN: DRXSY-D DRXSY-MP, H. Cohen
1	University of Wyoming ATTN: D.L. Boyer University Station Laramie, WY 82071		Commander, USATECOM ATTN: DRSTE-TO-F  Director, USACSL, Bldg. E3330, EA ATTN: DRDAR-CLN W. C. Dee
3	Virginia Polytechnic Institute and State University Department of Aerospace Engineering ATTN: Tech Library Dr. W. Saric Dr. T. Herbert Blacksburg, VA 24061		Director, USACSL, Bldg. E3516, EA ATTN: DRDAR-CLB-PA M. C. Miller DRDAR-CLJ-L DRDAR-CLB-PA DRDAR-CLN
1	Woods Hole Oceanographic Institute ATTN: J.A. Whitehead Woods Hole, MA 02543		

### USER EVALUATION OF REPORT

Please take a few minutes to answer the questions below; tear out this sheet, fold as indicated, staple or tape closed, and place in the mail. Your comments will provide us with information for improving future reports.

1. BRL Report Number \_\_\_\_\_

2. Does this report satisfy a need? (Comment on purpose, related project, or other area of interest for which report will be used.)

\_\_\_\_\_  
\_\_\_\_\_  
\_\_\_\_\_

3. How, specifically, is the report being used? (Information source, design data or procedure, management procedure, source of ideas, etc.) \_\_\_\_\_

\_\_\_\_\_  
\_\_\_\_\_

4. Has the information in this report led to any quantitative savings as far as man-hours/contract dollars saved, operating costs avoided, efficiencies achieved, etc.? If so, please elaborate.

\_\_\_\_\_  
\_\_\_\_\_

5. General Comments (Indicate what you think should be changed to make this report and future reports of this type more responsive to your needs, more usable, improve readability, etc.) \_\_\_\_\_

\_\_\_\_\_  
\_\_\_\_\_  
\_\_\_\_\_

6. If you would like to be contacted by the personnel who prepared this report to raise specific questions or discuss the topic, please fill in the following information.

Name: \_\_\_\_\_

Telephone Number: \_\_\_\_\_

Organization Address: \_\_\_\_\_

\_\_\_\_\_  
\_\_\_\_\_